THE ROLE OF AN OPTIMAL MODELING BASIS IN VARIATIONAL RESOLVENT ANALYSIS

Benedikt Barthel
Graduate Aerospace Laboratories
California Institute of Technology
1200 E California Blvd, Pasadena CA, 91125
bbarthel@caltech.edu

Salvador Gomez
Graduate Aerospace Laboratories
California Institute of Technology
1200 E California Blvd, Pasadena CA, 91125

Beverley J. McKeon
Graduate Aerospace Laboratories
California Institute of Technology
1200 E California Blvd, Pasadena CA, 91125

ABSTRACT

This work is concerned with the variational formulation of resolvent analysis (VRA) introduced by Barthel *et al.* (2022). In this framework, resolvent modes are approximated by projecting onto a lower dimensional modeling basis. There are no inherent restrictions on this basis, but in general the efficacy of the model relies on a priori knowledge of the spatial support of the modes of interest. We apply the VRA framework to a a (1D) Ginzburg-Landau model as well as a (2D) streamwise developing mean flow to investigate the effect of the boundary conditions of the modeling basis on the accuracy of the VRA approximation. For the latter we employ a modeling basis of local (1D), and thus streamwise periodic, resolvent modes. We find that for weak to moderate streamwise development of the background flow the periodic basis functions provide accurate approximations of the global modes. However, as the streamwise dependence of the background flow grows, the VRA approximation degrades.

1 Introduction

Resolvent analysis (RA) can be used to give insight into the forced response of a linearized dynamical system. This concept was introduced by Trefethen *et al.* (1993) and Jovanović & Bamieh (2005) who considered the stability and amplification of linearly stable flows to external forcing. These ideas were later applied to turbulent flows by McKeon & Sharma (2010) who interpreted the nonlinear term in the Navier-Stokes equations (NSE) as a forcing to the linearized system. The conceptual framework of RA is inspired by control theory (CT), such that the resolvent operator, the inverse of the linearized operator, is interpreted as a transfer function from the forcing to the response. A singular value decomposition (SVD) of the discretized resolvent operator provides two distinct orthonormal bases (left and right singular modes) for both the response and the forcing, ordered by a set of gains (singular values) which quantify the linear amplification of the system.

In this work we take an alternative approach and propose an equivalent definition based on the calculus of variations. In this definition introduced by Barthel *et al.* (2022), the resolvent response modes are defined as stationary points of the operator norm of the linearized dynamics. The variational formulation discussed here constitutes an extension from the min-max principle principle which concerns only the optimal resolvent mode, to what Barthel *et al.* (2022) coined "variational resolvent analysis" (VRA) which concurrently defines all resolvent modes.

This variational definition is based on the solutions of the Euler-Lagrange equations associated with the constrained variation of the operator norm of the linearized dynamics. Critically, this definition does not involve the inversion of any operator, which is useful from both a theoretical and practical sense. The inversion of large matrices is both costly and obscures the intuitive interpretation of the underlying linear differential operator. While in general the resulting Euler-Lagrange equations remain difficult to solve exactly, this variational formulation allows for the approximation of resolvent modes as an expansion in any convenient basis, for example the much cheaper one-dimensional resolvent basis in a two- or three-dimensional problem, an analytical basis such as that described by Dawson & McKeon (2019) or a data-driven one. Further, it requires only the eigenvalue decomposition of a matrix of reduced size. In this sense the freedom to choose a convenient modeling basis is both a strength and a weakness, as it allows for greater flexibility, but places the burden of choosing an efficient basis on the user. In order to provide any practical advantage, the modeling basis should be small compared to the dimension of the full system, however it must be large enough to (reasonably) span the modes being modeled. While in many cases physical mechanisms such as localization about a critical layer or symmetries such as periodicity within a domain can guide the choice of modeling basis, this may not always be the case. In this paper we expand on the results of Barthel *et al.* (2022) and investigate in more detail the limitations of the variational approximation of global resolvent modes when the boundary conditions of the modeling basis do not match those of the linear operator under investigation.

2 A variational definition of resolvent modes

As described by Barthel *et al.* (2022), the resolvent response modes may be defined as the stationary points, $\mathbf{q}^*$, of the operator norm of $\mathbf{L}$ under the condition that the argument $\mathbf{q}^*$ satisfies some norm constraint. More explicitly, the resolvent modes of the linear operator $\mathbf{H}$ are defined as the stationary points of the functional

$$J = \|\mathbf{L}\psi\|_a^2 \tag{1}$$

subject to the constraint

$$\|\psi\|_b^2 = 1 \tag{2}$$

where the norms $||\mathbf{x}||_a$ and $||\mathbf{x}||_b$ need not be the same. For simplicity, each norm $||\mathbf{x}||_i$ will be associated with the inner product $\langle \mathbf{a}, \mathbf{b} \rangle_i = \mathbf{a}^* \mathbf{Q}_i \mathbf{b}$, where $\mathbf{Q}_i$ is a positive definite matrix. The method of Lagrange multipliers allows us to formulate a constrained variational problem and define a Lagrangian

$$\mathscr{L}(\psi) = \psi^H \mathbf{L}^H \mathbf{Q}_a \mathbf{L}\psi - \sigma^{-2}\psi^H \mathbf{Q}_b \psi. \tag{3}$$

The resolvent response modes of $\mathbf{H} = \mathbf{L}^{-1}$ are then defined as the solutions to the Euler-Lagrange equations given by

$$\mathbf{L}^H \mathbf{Q}_a \mathbf{L}\psi_j = \sigma_j^{-2} \mathbf{Q}_b \psi_j. \tag{4}$$

The resolvent forcing modes are recovered through

$$\phi_j = \sigma_j \mathbf{L}\psi_j. \tag{5}$$

We would like to highlight a specific advantage of the proposed variational formulation in Equations 1 and 2. We note that the norms $\|\mathbf{x}\|_a$ and $\|\mathbf{x}\|_b$ norms need not only not be the same, they need not be quadratic. In many physical problems the norms of interest are not quadratic, such as in compressible flows where the temperature contributes a linear term in the total energy. This variational formulation presents a straightforward way to define a ‘resolvent basis’ in such cases. The SVD based definition is inherently limited to quadratic norms since in a practical sense it is based on the Euclidean 2-norm. However, in this paper we focus on quadratic norms to allow for the comparison of our methods to classical SVD based algorithms.

3 Estimation of Global Modes

In general, the Euler-Lagrange equations (4) are both analytically intractable and computationally intensive for complex flows with multiple non-homogeneous spatial dimensions. However, the variational definition provides a convenient way to estimate resolvent modes as an expansion in any convenient known basis: $\mathbf{q}_j(\mathbf{x})$ with $(j = 1...r)$. The global resolvent response modes may then be expanded as

$$\psi = a_j \mathbf{q}_j \tag{6}$$

which upon insertion into (3) transforms the continuous vector field $\mathbf{q} \in \mathrm{C}^\infty$ into a discrete field $\mathbf{a} \in \mathrm{C}^r$, where $\mathbf{a}$ is the vector of amplitudes a_j. The Euler-Lagrange equations then take the form of an eigenvalue problem

$$\mathbf{Ma} - \sigma^{-2}\mathbf{Qa} = 0, \tag{7}$$

where $\mathbf{M}, \mathbf{Q} \in \mathrm{C}^{r\times r}$. The eigenvectors $\mathbf{a}$ contain the amplitudes a_j which optimally approximate the resolvent response modes and the σ are the approximate singular values. Throughout the paper we use r to refer to the size of the reduced system (7) and n to refer to the size of the original system, and for large systems we achieve a model reduction, r/n, of up to two orders of magnitude. In this work we use analytical or 1D local resolvent modes as a modeling basis. However, other types of basis are possible, for example see Towne *et al.* (2015) for a discussion of using data as a modeling basis for global resolvent modes in the context of turbulent jets.

While the freedom to choose a modeling basis offers flexibility in the application of the VRA method, it also presents inherent limitation. Namely one may not know a priori what basis is optimal, or how many basis elements are required for satisfactory convergence. This is of particular concern when analyzing flows with non-periodic and non-homogeneous boundary conditions. For example, Barthel *et al.* (2022) found that when the boundary conditions of the modeling basis $\mathbf{q}_j$ differed significantly from the natural boundary conditions of the linear operator $\mathbf{L}$, the accuracy of the VRA approximation deteriorated. Those authors used streamwise periodic local resolvent modes as a modeling basis for global modes for a streamwise developing boundary layer. They found that when the global modes under investigation were localized close to the wall, and thus not significantly affected by the streamwise development of the mean flow, the streamwise periodic modeling basis led to accurate reconstructions. However, when the global modes extended into the wake region, and thus subject to the strong streamwise development of the mean flow, the VRA approximation deteriorated.

4 Ginzburg-Landau Model

To investigate the effects of using a modeling basis with suboptimal boundary conditions we apply the VRA to the simple case of the Ginzburg-Landau (GL) equation, in particular, the case studied in Bagheri *et al.* (2009). Here, we denote the linear operator

$$\mathscr{A} = -i\omega + \mathscr{L} = -i\omega - \nu\partial_x + \gamma\partial_x x + (\mu_0 - c_\mu^2) + \frac{\mu_2}{2}x^2, \tag{8}$$

and the resolvent operator, $\mathscr{H} = \mathscr{A}^{-1}$ for $x \in \mathbb{R}$, assuming compact support. The coefficients ν, γ, μ_0, and c_μ are chosen to be the same as in Bagheri *et al.* (2009). Here the frequency, ω is set to 2 and μ_2 is either -0.01 or 1. Finally, the standard inner product over $\mathbb{R}$ is chosen such that

$$\langle a, b \rangle = \int_{-\infty}^{\infty} a^*(x) b(x) dx. \tag{9}$$

As noted by Cossu *et al.* (2009), the GL equation has many of the hallmarks of the problems studied in wall bounded shear flows, namely the convective nonnormality and nonparallel effects, paramaterized by the coefficients ν and μ_2, respectively. By varying μ_2 between -0.01 and -1 we can model the effect of increased nonparallel terms in the operator on the choice of modelling basis.

This operator is discretized to create a matrix representation, with $\mathbf{A}$ and $\mathbf{H}$ being the discretized versions of $\mathscr{A}$ and $\mathscr{H}$, respectively. Differentiation is performed with fourth-order central difference schemes using $N = 1920$ equispaced grid points for $x \in [-L, L]$ with $L = 50$. Dirichlet boundary conditions are enforced in $\mathbf{A}$. Integration is performed with a trapezoidal-rule integration scheme, which is enforced through the diagonal, positive definite matrix $\mathbf{W}$. As such, the inner product is discretized such that

$$\langle \mathbf{a}, \mathbf{b} \rangle = \mathbf{a}^* \mathbf{W} \mathbf{b}. \tag{10}$$

Although $\mathbf{A}$ is sparse, the required matrix operations for resolvent analysis scale with $\mathscr{O}(N^3)$.

To investigate the role of the boundary conditions, we will illustrate the VRA with two sets of modeling basis elements. The first set of basis elements will be created with Gaussians, centered at different locations. The basis is defined as

$$\mathbf{b}_j^G(x; r) = \frac{1}{\sqrt{2\pi\sigma_r^2}} \exp\Big(\frac{(x - x_{r,j})^2}{2\sigma_r^2}\Big), \tag{11}$$

where r denotes the number of basis elements. Here, $\sigma_r = \frac{2L}{.675r}$ and $x_{r,h} = \frac{2L}{r} j - L$, so that the width and location of the Gaussians depend on the number of basis elements. The second set of basis elements are chosen to be Fourier modes such that

$$\mathbf{b}_j^F(x; r) = \frac{1}{\sqrt{L}} \exp\Big(ij\frac{2\pi}{L}x\Big). \tag{12}$$

Note that the Fourier basis does not have compact support in all the basis elements, unlike the Gaussian basis.

In Figure 1, the singular values from the VRA approximation are compared with the SVD based modes using 23 basis elements with $\mu_2 = -0.01$. The blue triangles denote the singular values from the Gaussian basis, the red circles denote the singular values from the Fourier basis, and the black circles are the singular values from the SVD. Note that the convergence is best for the leading singular values and drops off for the higher order modes, which is consistent with Barthel *et al.* (2022).

In Figure 2, the response modes and the forcing modes are plotted to compare the approximation of the resolvent modes using 23 basis elements for $\mu_2 = -0.01$. The colors are the same as in Figure 1 and here only the leading four response and forcing modes are plotted. The forcing modes are computed using Equation 5. The error in the forcing modes is that the matrix $\mathbf{A}$ is not a directional amplifier in the direction of the leading forcing modes. Any error in the approximation of the response modes becomes amplified when computing the forcing modes.

Finally, the convergence of the singular values, response modes, and forcing modes for $\mu_2 = -0.01$ and $\mu_2 = -1$ is plotted in Figures 3 and 4, respectively. The error in the singular values is defined as $e_{\sigma,i} = |\sigma_i - \tilde{\sigma}_i|$, where $\tilde{\sigma}_i$ denotes the singular value approximated from the VRA in either basis. The error in the forcing modes and response modes is defined as $e_{\phi,i} = ||\phi_i - \tilde{\phi}_i||$ and $e_{\psi,i} = ||\psi_i - \tilde{\psi}_i||$, respectively. For $e_{\phi,i}$ and $e_{\psi,i}$, the norm denotes the induced norm from the inner product and the tilde denotes the approximate mode

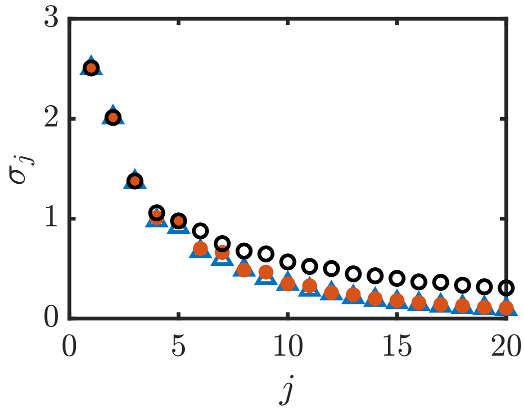

Figure 1: Comparison of singular values using 23 basis elements for the GL system with $\mu_2 = -.01$. The blue triangles and red dots are the VRA approximated singular values using a Gaussian basis and Fourier basis, respectively. The black open circles are the singular values computed using the SVD.

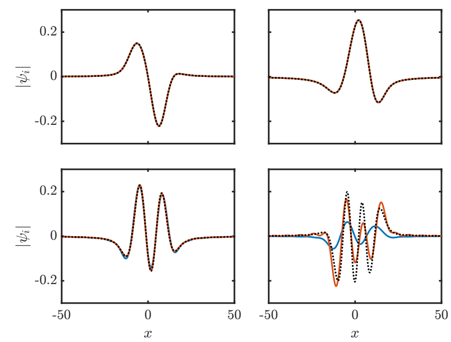

(a) Response modes

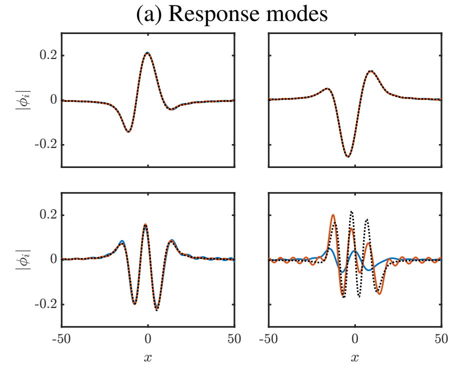

(b) Forcing modes

Figure 2: Comparison of response modes and forcing modes with 23 basis elements for the GL system with $\mu_2 = -0.01$. The solid lines are the VRA approximated modes using the Gaussian basis (blue) and the Fourier basis (red) while the dotted black lines are the SVD modes. For each subplot $j = 1-4$ from top left.

from the VRA approximation. In this case, the number of basis elements is varied, and generally, convergence increases with increasing number of basis elements. The closed circles denote the error with the Fourier basis, while the open triangles denote the error with the Gaussian basis. For larger number of basis elements, r, the Gaussian basis converges faster than the Fourier basis. The reason for this quick convergence is because

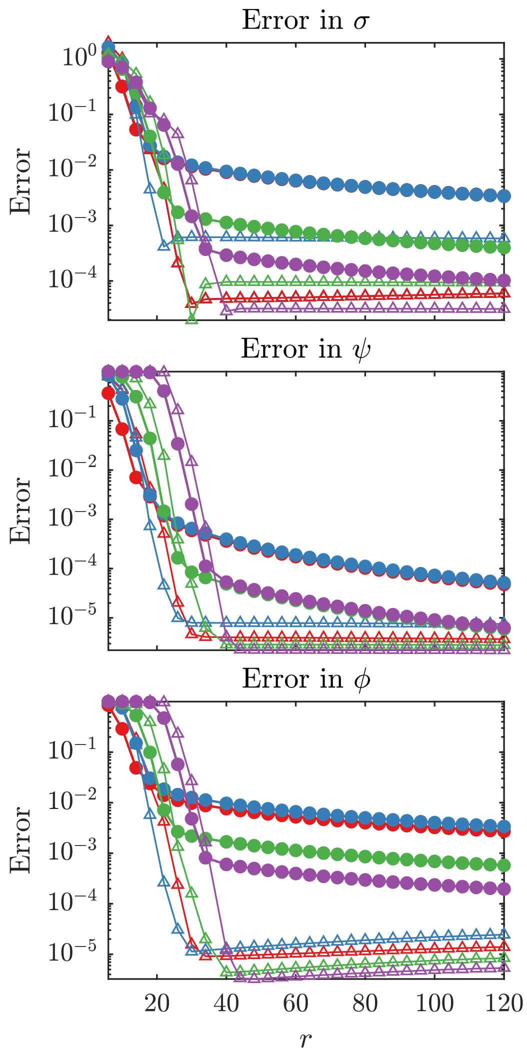

Figure 3: Error in the singular values, response modes, and forcing modes using r Gaussian basis elements (open triangles) or r Fourier basis elements (closed circles) for the GL system with $\mu_2 = -.01$. The red, blue, green, and purple denote the error in the 1st, 2nd, 3rd, and 4th mode, respectively.

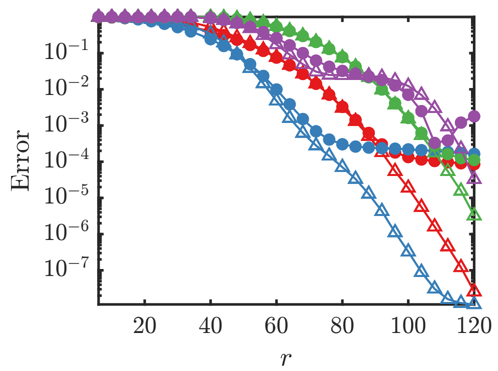

Figure 4: Error in the response modes using r basis elements, with the same markers as figure 3, for the GL system with $\mu_2 = -1$.

the Fourier basis is not compact whereas the resolvent modes of the Ginzburg Landau operator are. The broad support of the Fourier modes means that a large number of them are required to resolve the resolvent modes, which have compact support. This is similar to resolving a localized bump with a Fourier series. The Gaussian basis does not have this limitation and it is better able to resolve the modes. Comparing Figures 3 and 4, it is clear that the convergence in both bases is slower with the increase in μ_2. This decrease in convergence rate is likely due to the fact that the term $\frac{\mu_2}{2}x^2$ in Equation 8 acts as a potential well and increasing the magnitude of the coefficient makes the term stronger, effectively making the potential well thinner thereby making the resolvent modes narrower. These narrow modes pose problems for the Gaussian basis functions for small r, since their widths depends on r, but ultimately this basis can resolve these modes as shown in Figure 4. While the Fourier basis can resolve these modes, this basis is not as efficient for $\mu_2 = -1$ by the fact that the Fourier series is effectively resolving a more localized signal in space.

Finally, in Figure 3, the convergence of the forcing modes is slower than the convergence of the response modes because $\mathbf{A}$ amplifies the error in the approximation. Although not shown here, this is also the case for the forcing modes of $\mu_2 = -1$

5 Streamwise Developing Boundary Layer

Next we consider resolvent modes computed about a streamwise developing mean flow, the configuration investigated in Barthel *et al.* (2022). In this case the reference 2D resolvent modes are computed using the NS operator linearized about the 2-dimensional, 2-component (2D/2C) mean flow, $\bar{\mathbf{U}}(x,y)$ modelled with the Monkewitz composite profile (Monkewitz *et al.*, 2007) with inlet friction Reynolds number $Re_\tau = 1200$. The modes are parameterized by the spanwise wavenumber k_z and the temporal frequency, ω, which are defined with respect to inlet δ_{99} and free stream velocity.

The global reference modes are computed using Chebyshev collocation in the wall normal direction and Fourier differentiation in the streamwise direction. The natural boundary conditions relevant to the fluctuations of the state $\mathbf{q} = [u,v,w,p]^T$ about the spatially developing mean velocity are: $\mathbf{u}(x,0) = \mathbf{0}$, $v_y(x,y) = 0$, and $\mathbf{u}_y(x,y_{max}) = \mathbf{0}$. An artificial sponge layer is applied to damp any artificial reflections due to the boundary conditions as in Ran *et al.* (2017, 2019), which also has the effect of damping the modes in this region and relaxes the periodic constraint on the modes. This is in contrast to the modeling basis of 1D resolvent modes, computed using the inlet mean velocity, $q_j(x,y) = \psi_j^{1D}(y;k_x,k_z,c)e^{ik_x x}$, which are periodic in the streamwise direction and have support across the entire domain. The reference modes are computed using an LU decomposition and Arnoldi Method which is applied as in Sipp & Marquet (2013) and Schmidt *et al.* (2018) to compute the SVD of the resolvent by solving linear systems, as opposed to computing the matrix inverse. See Barthel *et al.* (2022) for a more details of both the modeling basis as well as the numerical strategies used to compute the reference modes.

We show the results for three wavenumber - frequency combinations, $[k_z,\omega] = [301, 5.6]$, $[75, 2.8]$, and $[2\pi, 1.9]$. he ratio of the number basis elements to the degrees of freedom in the fully discretized system is $1/288$, $5/648$, and $5/432$, respectively, a reduction by two orders of magnitude. These modes exhibit support over an increasing wall-normal extent and are thus increasingly affected by the wake development of the mean velocity. This allows us to to illustrate how the increasing streamwise development of the mean flow affects the accuracy of the VRA reconstruction using the streamwise periodic modeling basis. We will refer to the results from these combinations as short, medium, and tall, respectively.

The VRA approximation of the first two resolvent response modes is compared to the SVD-based reference in Figure 5. The short modes, in Figures 5a and 5b, are localized near the wall extending only up to approximately $y^+ = 30$. In this region, the flow is essentially parallel which makes the Fourier (in x) modeling basis a nearly optimal choice to model these short modes and results in a VRA approximation that is almost indistinguishable from the reference mode.

The medium modes, shown in Figures 5c and 5d, extend further, up to about $y^+ = 100$, these modes begin to exhibit signs of non-periodicity in the streamwise direction. In this case the Fourier modeling basis is no longer capturing the exact boundary conditions of the reference modes. However, the error in the VRA approximation is largely confined to the streamwise boundaries of the domain. In the bulk of the domain the VRA approximation captures the qualitative, and quantitative features of the reference. It is interesting to note that the support of the VRA approximation is generally shifted slightly upstream relative to the reference. The VRA modes tend to be roughly centered in the domain, while the reference is increasingly concentrated towards the downstream side as the streamwise development strengthens.

Finally, we plot the tall modes in Figures 5e and 5f. These modes have support all the way to approximately $y^+ = 500$ and are thus strongly affected by the streamwise development of the mean flow. Here the downstream bias of the reference mode is even more pronounced, with the bulk of the modes amplitude being in the downstream half of the domain. The VRA approximation largely fails to capture this asymmetry, displaying support throughout the domain. Despite this, we note that the VRA approximation does capture the amplitude and the fundamental streamwise wave number observed in the reference mode.

The VRA approximation recovers the near wall modes more faithfully than the taller modes. Part of this can be attributed to the increase in nonparallel effects of the mean as distance from the wall is increased. This can serve as an analogy to what was observed in the case of the GL operator with increase in $|\mu_2|$ since this parameter increased the nonparallel terms in the GL operator. On the other hand, the effect of the distance from the wall does not constrain the spatial support of the modes like in the GL case. Nonetheless, the choice of modelling basis for this operator is suboptimal because of the significant streamwise variation in the mean and the presence of nonreflecting boundary conditions that limit the periodicity assumed in the basis elements. In particular, this can be gleaned by noting that the true global modes in Figures 5e and 5f abruptly decay to 0 at around $x = 32$ because of the sponge. This abrupt decay behaves like a Heaviside function, which requires a lot of Fourier modes to resolve. On the other hand, for the near wall modes, these modes had already begun to decay due to viscous dissipation downstream so the effect of the sponge setting the modes to 0 is minimal.

6 Summary

In this work we investigated the impact of the modeling basis on the efficacy of the variational resolvent analysis modeling of global resolvent modes introduced by Barthel *et al.* (2022). This approach is susceptible to errors when there is sufficient mismatch between the boundary conditions of the modeling basis and the linear operator whose resolvent modes are being modeled. We illustrated this phenomenon through the analysis of a Ginzburg-Landau model and found that modeling basis which satisfy the proper boundary conditions lead to drastically improved convergence properties. We also applied the VRA approach to the NSE governing the fluctuations about a streamwise developing boundary layer flow. In this case the VRA approximation using a streamwise periodic modeling basis is very effective in modeling near wall modes, but deteriorates as the global modes being modeled extend further into the wake region of the boundary layer.

We acknowledge funding from ONR grants numbers: N00014-17-1-2307 and N0014–17–1-3022.

REFERENCES

Bagheri, Shervin, Henningson, Dan S, Hoepffner, J & Schmid, Peter J 2009 Input-output analysis and control design applied to a linear model of spatially developing flows. *Applied Mechanics Reviews* **62** (2).

Barthel, Benedikt, Gomez, Salvador & McKeon, Beverley J. 2022 Variational formulation of resolvent analysis. *Physical Review Fluids* **7** (1), 013905.

Cossu, Carlo, Pujals, Gregory & Depardon, Sebastien 2009 Optimal transient growth and very large–scale structures in turbulent boundary layers. *Journal of Fluid Mechanics* **619**, 79–94.

Dawson, Scott T. M. & McKeon, Beverley J. 2019 On the shape of resolvent modes in wall-bounded turbulence. *Journal of Fluid Mechanics* **877**, 682–716.

Jovanović, Mihailo R. & Bamieh, Bassam 2005 Componentwise energy amplification in channel flows. *Journal of Fluid Mechanics* **534**, 145–183.

McKeon, Beverley. J. & Sharma, Ati. S. 2010 A critical-layer framework for turbulent pipe flow. *Journal of Fluid Mechanics* **658**, 336–382.

Monkewitz, Peter A, Chauhan, Kapil A & Nagib, Hassan M 2007 Self-consistent high-reynolds-number asymptotics for zero-pressure-gradient turbulent boundary layers. *Physics of Fluids* **19** (11), 115101.

Ran, Wei, Zare, Armin, Hack, M. J. Philipp & Jovanović, Mihailo R. 2019 Stochastic receptivity analysis of boundary layer flow. *Physical Review Fluids* **4** (9), 093901.

Ran, Wei, Zare, Armin, Nichols, Joseph W. & Jovanovic, Mihailo R. 2017 The effect of sponge layers on global stability analysis of Blasius boundary layer flow. In *47th AIAA Fluid Dynamics Conference*. American Institute of Aeronautics and Astronautics.

Schmidt, Oliver T., Towne, Aaron, Rigas, Georgios, Colonius, Tim & Brès, Guillaume A. 2018 Spectral analysis of jet turbulence. *Journal of Fluid Mechanics* **855**, 953–982.

Sipp, Denis & Marquet, Olivier 2013 Characterization of noise amplifiers with global singular modes: the case of the leading-edge flat-plate boundary layer. *Theoretical and Computational Fluid Dynamics* **27** (5), 617–635.

Towne, A., Colonius, T., Jordan, P., Cavalieri, A. V. & Brès, G. A. 2015 .

Trefethen, Lloyd N., Trefethen, Anne E., Reddy, Satish C. & Driscoll, Tobin A. 1993 Hydrodynamic Stability Without Eigenvalues. *Science* **261** (5121), 578–584.

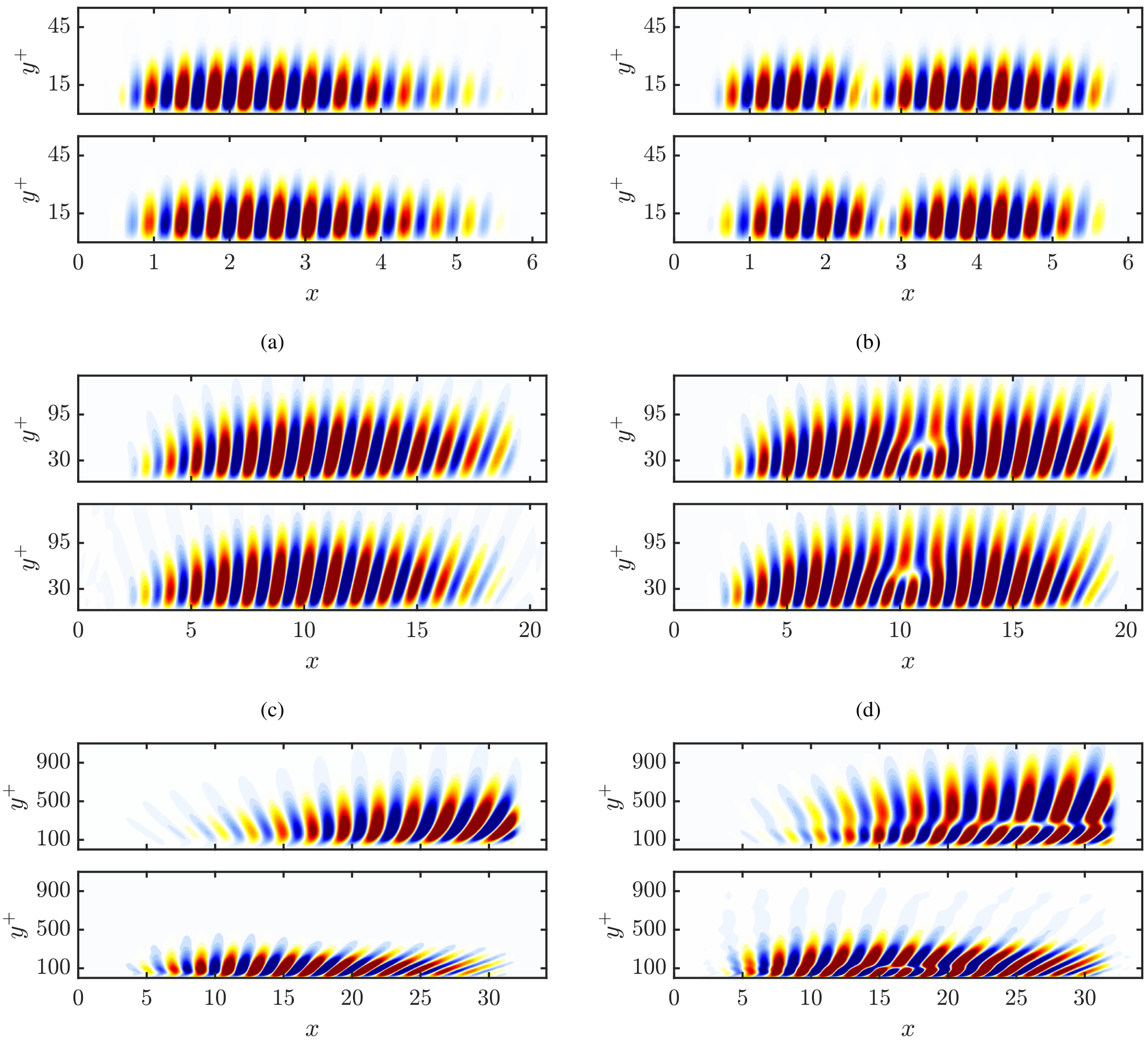

Figure 5: First two resolvent response modes (ψ_j). Real part of the streamwise component u, $j = 1$ (left column), and $j = 2$ (right column). $[k_z, \omega] = [301, 5.6]$ (a, b), $[75, 2.8]$ (c, d), $[2\pi, 1.9]$ (e, f). Top panels: true global modes, bottom panels: VRA model. lower x-axis represents outer units x.